3 CHAPTER

ADAPTIVE NOISE ESTIMATOR FOR THE APPLICATIONS OF DE-NOISING AND SEGMENTATION OF MRI DATA

Highlights of the Chapter

- *Present chapter proposes an algorithm for adaptive noise estimation based on multi-objective particle swarm optimization (MOPSO)*
- *MOPSO based non-local Kalman filter and MOPSO based linear minimum mean square error (LMMSE) filter to de-noise the MRI data*
- *Adaptive noise estimation technique has been found valuable for recursive and non-recursive filters both*

Abstract

The present study proposes the noise estimation of Magnetic Resonance Imaging (MRI) data using multi-objective particle swarm optimisation (MOPSO). This adaptive noise estimation is based on the maximisation of the multiple quality measures, which enable the algorithm to achieve de-noising along with enhancement in the image features. The chapter proposes two filtering approaches to de-noise MRI data. In first, MOPSO based noise estimation is followed by non-local statistics based Kalman filter, whereas, in the second approach,

MOPSO based noise estimation is followed by Linear Minimum Mean Square Error (LMMSE) filter. The impact of de-noising on segmentation of MRI data has also been studied, for this purpose enhanced fuzzy c-means algorithm has been applied on filtered MRI data. The de-noising and segmentation performance of MOPSO-non local Kalman filter and MOPSO-LMMSE filters has been evaluated and compared with Wavelet filter, Wiener filter, non-local mean filter, standard Kalman and standard LMMSE filter. The proposed noise estimation approach followed by filtering is giving better de-noising and segmentation results as compared to standard filters considered.

3.1 Introduction

MRI is an important modality of medical imaging as far as concern the structure of soft tissues, their details and disease characterisation. The advantages of this imaging technique are its non-ionization behaviour and better image quality with high tissue contrast resolution. This imaging technique produces different weighted images by varying in the sequences of radio frequency (RF) pulses, and these weighted sequences can be used to diagnose the various diseases [110, 111]. However, the presence of artifacts and noise in the MRI data may affect the perception of the radiologists. Hence, an efficient de-noising as a pre-processing step should be implemented [14].

Previously, many filtering algorithms have been proposed to de-noise MRI data [37, 112]. The conventional Wiener filters [113] are simple and process the local neighbourhood pixels. However, these filters assume Gaussian rather Rician distributed noise and hence often produce blur on resulting MRI data. An alternative to conventional Gaussian filtering, the approach based on Markov Random Field has the capability to preserve the shape of

transitions in fMRI studies [114]. Recently, Fabio Baselice et al. have exploited the Markov Random Field for de-noising and edge preservation of 3D MRI data, and tunes the parameters by itself [115]. The transformation-based de-noising method utilises Wavelet-based filter [116], which has improved the visual appearance of diffusion-weighted MRI data as it preserves the edges and reduces the blur. The non-local means (NLM) filter [24] has shown elegant accuracy in preserving the edges, which averages the non-local pixels of the image while considering the self-similarity property that determines the weights. Further, the idea of NLM filter has been extended to other de-noising methods as well [25, 117].

The recent trends are toward statistical estimation based de-noising approach for MRI data, which utilises quasi-Monte Carlo estimation has been instigated while considering local statistics of MRI data [118]. The maximum likelihood estimation method has been implemented in a non-local manner to de-noise the MRI data generated from multiple coils [26]. Jose V. Manjon et al. estimated the noise level of the MRI data followed by de-noising using non-local principle component analysis (PCA) [25]. Further, linear minimum mean square error (LMMSE) based techniques are another class of de-noising method and have the ability to produce a greater de-nosing performance. S. Aja-Fernandez et al. proposed an iterative LMMSE approach for signal estimation in MRI data [27]. This LMMSE estimation based approach has been implemented on the local statistics of the data. Later on, the LMMSE approach has been exploited for non-local statistics for the 3D MRI data to obtain enhanced performance [119]. Apart from LMMSE, other filters such as patch based PCA filter have also used an iterative approach [120]. These iterative filtering approaches assume the Rician distribution of MRI data at every iteration, however, the nature of resulting data changes after each iteration. Further, signal estimation based on non-recursive Kalman filter

has been applied earlier to photographic images using local statistics for the enhancement of contrast and de-noising [121]. This work has performed de-noising without doing noise estimation, and hence, direct application of this standard Kalman filter it is not found very suitable for the de-noising of MRI data. V. Brion et al. proposed the parallel Kalman filter for real-time χ-noise correction of diffusion tensor imaging and High Angular Resolution Diffusion Imaging data [122]. Recently, a modified Kalman filter has been used, where Markov random field has been followed by a standard Kalman filter to de-noise the image [123].

The present chapter implements MOPSO for noise estimation followed by de-noising algorithms, i.e. LMMSE based filter and modified Kalman based filter. The present study suggested that the noise need to be adaptively estimated in the process of filtering of MRI data. The previous recursive filtering methods have assumed MRI data as Rician distributed throughout all the iterations. However, the Rician nature of MRI data get modified after each iteration. Hence, adaptive estimation of noise after each iteration is a primary requirement of the filtering. The non-recursive filters also get benefited from proposed approach, as MOPSO objectively maximizes the image quality parameters to estimate the noise from MRI data. Further, enhanced fuzzy c-means segmentation algorithm [124] also shows better segmentation results with proposed algorithms. The rest of the chapter is organized as follows. The next section describes the problem formulation to estimate the noise. Section 3.3 formulates the non-local Kalman filter to de-noise the MRI data. Section 3.4 presents the material and proposed algorithm along with its working. Section 3.5 demonstrates the experiment results, and finally, Section 3.6 concludes the study.

3.2 Problem formulation

The complex-valued MRI data is reconstructed from the inverse Fourier Transform of k-space data and contains white Gaussian noise [125]. The magnitude MRI data follows the Rician distribution [22], as computation of magnitude MRI from complex-valued MRI data is a non-linear mapping process. The magnitude signal, which is the envelope of the complex signal can be expressed as follows:

$$M(x) = |A(x) + N(x)| \tag{3.1}$$

where $A(x)$ is noise free amplitude data and $N(x) = n_{Re}(x) + i\, n_{Im}(x)$ is the complex white Gaussian noise having zero mean, n_{Re}: a real component of $N(x)$and n_{Im}: the imaginary components of $N(x)$. The probability density function (PDF) of M can be expressed as Rician and represented as follows [126]:

$$p_M(M|A,\sigma_n) = \frac{M}{\sigma_n^2}\exp\left(-\frac{M^2+A^2}{2\,\sigma_n^2}\right) I_0\left(\frac{A\,M}{\sigma_n^2}\right) \tag{3.2}$$

where σ_n^2 is noise variance and $I_0(x)$ is the first kind 0^{th} order Bessel function. As there is no signal in the background of the MRI data, the PDF of Rician can be converted to the Rayleigh distribution in this region [127], which is computed by putting $A = 0$ in the Equ. (3.2) and is expressed as follows:

$$p_M(M,\sigma_n) = \frac{M}{\sigma_n^2}\exp\left(-\frac{M^2}{2\,\sigma_n^2}\right) \tag{3.3}$$

3.2.1 Estimation of noise variance

Previously, the estimation of noise variance (σ_n^2) has been derived while using the background (or non-signal region) of the magnitude MRI, such as: the simple estimator based

on method of moments has been proposed [128], which is given as $\widehat{\sigma_n^2} = \frac{1}{2}\langle M^2 \rangle$, where $\langle\ .\ \rangle$ is sample estimator, M^2 is second order moment, and hence, $\langle M^2 \rangle$ is sample second order moment. Sijber J et al. has been estimated $\widehat{\sigma_n}$ in the non-signal region, defined as: $\widehat{\sigma_n} = \sqrt{\frac{2}{\pi}}\langle M \rangle$ [129], where $\langle M \rangle$ is sample mean. In another study, the noise has been estimated for Rician distribution expressed as $\widehat{\sigma_n^2} = \frac{1}{2}\left(\langle M^2 \rangle - (2\langle M^2 \rangle^2 - \langle M^4 \rangle^{1/4}\right)$ [130]. Recently, a very efficient noise estimation methods have been suggested, which is based on the maximum distribution of sample local statistics [27], and is defined as $\widehat{\sigma_n} \approx \frac{\sqrt{e}}{2}\ mode\ (\mu_{1_{ij}})$, where $\mu_{1_{ij}}$ is local mean.

The above-discussed approaches were proposed for Rician distribution of MRI data. However, in the process of filtering of MRI data, the recursive filters modify its Rician distribution after the first iteration, which results in non- Rician distribution of data in subsequent iterations [27]. Hence, there is a need for adaptive re-estimation of noise level after each iteration. Further, it is observed that the different values of the constant factor $\sqrt{\frac{1}{2}} \approx 0.707, \sqrt{\frac{2}{\pi}} \approx 0.797, and\ \frac{\sqrt{e}}{2} \approx 0.824$ has been proposed in literatures [128-130] to estimate the $\widehat{\sigma_n}$. The noise estimation was based on the assumption that there is no bias field present in the data, however, there is the probability that bias field may be present in real MRI data. In the view of above reasons, the present study proposes the MOPSO based noise estimation approach.

Instead of a fixed value of constant factor in noise estimation, MOPSO selects the value of this factor adaptively. Hence, the expression of noise estimation can be defined as follows:

$$\hat{\sigma}_{opt} \approx k \; mode \; \langle \widehat{\mu_{1_{ij}}} \rangle \tag{3.4}$$

where MOPSO randomly initialises the constant factor k within the search space and searches its optimum position for the maximization of two objectives i.e. image quality measures PSNR and image anisotropy quality index (AQI) [131].

The proposed noise estimation approach is further helpful in adaptive design of recursive as well non-recursive filters for de-noising and enhancement of MRI data effectively. The de-noising of the image can be quantified in terms of structure similarity index (SSIM), peak signal to noise ratio (PSNR) image quality based on local variance (IQLV) [132] and AQI. Previously, image qualities PSNR, AQI and IQLV has been found valuable to quantify the enhancement and de-noising [133-135], hence, the present study has chosen to adopt these image quality indexes. The higher value of these image quality measures represents the lower noise and better enhancement of the image.

3.2.2 Multi-objective Particle Swarm Optimization (MOPSO)

MOPSO belongs to computational intelligence, which efficiently addresses complex problems. Recently, optimization algorithms have been used for the enhancement of MRI data [133, 136]. Particle Swarm Optimization (PSO) is one of the most popular evolutionary algorithm [137], developed by the R. C. Elbert and J. Kennedy [94].The swarm of particles moves toward the optimum solution over the search space using an iterative process. The particles keep tracking its coordinates in the solution space, which is associated with the objective function, called personal experience. Additionally, particles keep tracking the whole population for a global experience. In every iteration, the movement of the particles depends on its previous direction $v_i(t)$, previous position $x_i(t)$, personal best experience

$P_i(t)$ and the global best experience $G(t)$ whereas the position of particles decided by its last position and current direction. The following equations describe this situation as follows:

$$v_i(t+1) = w\ v_i(t) + r_1 c_1\ [P_i(t) - x_i(t)] + r_2 c_2\ [G(t) - x_i(t)] \quad (3.5)$$

$$x_i(t+1) = x_i(t) + v_i(t+1) \quad (3.6)$$

where t is the number of iteration, w denotes the inertia weight to balance the exploration and exploitation of the search space, are the random numbers distributed in the range of $[0,1]$, and c_1, c_2 are the positive constants called acceleration coefficients regulate the influence of personal experience and global experience respectively.

The aim of multi-objective optimization algorithm is to search for the set of solutions rather one solution. These solutions are called Pareto front, where no solution dominate other against all objective functions. The obtained non-dominant solutions are typically stored in an archive. This archive gets updated in each iteration depending upon the dominance relationship between the new solution and already stored solutions explained in [79]. In present study different sets of MOPSO parameters have been considered. The parameters that are giving best results for present case are reported in Table 3-1.

Table 3-1: Controlling parameters of MOPSO

Parameter	Value
Maximum number of iterations T_{max}	25
Size of Population	20
w	0.4 - 0.9
c_1, c_2	1.2, 1.2
Optimization variable	$\hat{\sigma}_{opt}$
Objective functions	PSNR, and anisotropy

3.2.2.1 Objective functions

This study maximises the two objective functions contains two different image quality measures i.e. PSNR, and AQI [131]. The maximisation of the first objective function i.e. PSNR ensures minimisation of noise, and the maximisation of second objective function i.e. AQI ensures the minimisation of blur and maximization of information content in the MRI data. The expression of these objective functions are given as follows:

$$f_1(k) = 10\log\left(\frac{max_I^2}{MSE}\right) \tag{3.7}$$

where max_I is the maximum pixel value of the image and $MSE = \frac{1}{nm}\sum_{i=1}^{n}\sum_{j=1}^{n}[I(i,j) - I_o(i,j)]^2$, $I(i,j)$ is Rician distributed noisy MRI data and $I_o(i,j)$ is the reference or ground truth MRI data.

$$f_2(k) = \sqrt{\frac{\sum_{s=1}^{S}[\mu - \sum_n R_s(n,\theta_L)/M]^2}{L}}, \tag{3.8}$$

where $R_3[n,\theta_L]$ is the Renyi's entropy for $\alpha = 3$, θ_L represents L orientations to measure the entropy.

The searching process of MOPSO based noise estimation followed by de-noising produces the images equal to the number of non-dominate solutions. Hence, this study selects the best image from the set of non-dominant solutions with the help of another image quality measure based on local variance (IQLV) [132]. This image quality measure evaluates the quality of structure and is sensitive to the blurring. In this way, the algorithm achieves the de-noised MRI data having minimum blurring and maximum information content. The present work implements MOPSO based noise estimation followed by Kalman filter is given in Section 3 for de-noising of MRI data.

3.3 De-noising of MRI data using non-local Kalman filter

Kalman has described the filter using state space approach [138], which enables the Kalman filter to employ as a predictor or smoothing filter. The present study utilises the Kalman filter for the de-noising of MRI data and assumes the form of data within a process as follows:

$$I(m,n) = w_1(m,n)\, I_o(m,n) + w_2(m,n) \tag{3.9}$$

where $w_1(m,n)$and $w_2(m,n)$ are independent white noises, and $I_o(m,n)$ is noise free original/ground truth image. This study follows the optimal linear approximation of equation (3.9) [121], which helps to construct the de-noising algorithm and derived as follows:

$$I'(m,n) = \langle w_1(m,n)\rangle\, I_o(m,n) + \langle I_o(m,n)\rangle[w_1(m,n) - \langle w_1(m,n)\rangle] + w_2(m,n) \tag{3.10}$$

A priori mean and variance of $I_o(m,n)$ can be defined with the help of equation (3.9), given as follows:

$$\langle I_o(m,n)\rangle = \frac{\langle I(m,n)\rangle - \langle w_2(m,n)\rangle}{\langle w_1(m,n)\rangle} \tag{3.11}$$

moreover, $Q(m,n) = \frac{var[I(m,n)] + I^2(m,n)}{\sigma_2^2 + \langle w_1^2(m,n)\rangle} - \langle I_o^2(m,n)\rangle - \sigma_1^2$ (3.12)

where $var[I(m,n)]$ is the local variance of the $I(m,n)$. The present study approximate $\langle I_o(m,n)\rangle$ by non-local means MRI data $I_{NLM}(m,n)$. Equations (3.10), (3.12) and $I_{NLM}(m,n)$ used to derive final Kalman estimator, is given as follows:

$$\hat{I}_o(m,n) = \langle I_{NLM}(m,n)\rangle + k(m,n)[I(m,n) - \langle w_1(m,n)\rangle \langle I_{NLM}(m,n)\rangle - \langle w_2\rangle] \tag{3.13}$$

where $k(m,n) = \frac{\langle w_1(m,n)\rangle\, Q(m,n)}{\langle I^2(m,n)\rangle \sigma_2^2\, \langle w_1^2(m,n)\rangle\, Q(m,n) + \sigma_1^2}$.

3.4 Experimental material and algorithm

The present study proposes a framework, which consist of two de-noising approaches. These approaches are: (i) MOPSO based noise estimation followed by LMMSE (MOPSO-LMMSE) and (ii) MOPSO based noise estimation followed by non-local Kalman filter based signal estimation (MOPSO-NL-Kalman). The pseudo code is illustrated in **Algorithm 3**. The given algorithm works as a first approach, if MOPSO-LMMSE de-noises the image and calculates the objective functions. On the other hand, the algorithm works as a second approach, if MOPSO-NL-Kalman de-noises the image and calculates the objective functions. The present framework has been tested and validated on simulated T1 weighted and T2 weighted MRI data. The ground truth MRI data in the size of 217×181 has been obtained from BrainWeb (www.bic.mni.mcgill.ca/brainweb/). Further, the Rician distributed noisy data has been obtained when ground truth MRI data has been added with complex Gaussian noise σ_n followed by calculation of magnitude MRI [139]. The experiment has considered wide range of noise $\sigma_n = 5, 7.5, 10, 12.5, 15, 17.5, 20$ added to the ground truth data.

The de-noised image has the application in improved diagnosis, manually and automatically both. Hence, the effectiveness of de-noising algorithm has been quantified not only in terms of visual image quality but also in terms of the segmentation quality. The image quality measures, i.e. PSNR, anisotropy and IQLV have been used to evaluate the quality of the filtered image. Further, the resultant output de-noised the enhanced fuzzy c-means segmentation [124] has been performed on the filtered MRI data, and the results have been quantified in terms of Jaccard similarity [140] and Dice coefficient [141].

Algorithm 3: MOPSO based noise estimation and de-noising of MRI data

Initialize the PSO parameters as shown in Table 3-1

*Randomly initialize the position of the particles (**k** in the present study, as shown in equation (3.4) within the limit of search space*

for** every particle in the population **do

Compute both objective functions as expressed through equations (3.7) and (3.8)*

end for

Create a Pareto front and store non-dominant solutions

Randomly initialize the personal best for every particle

for** t=1 to predefined maximum number of iterations T_{max} **do

for** every particle in the population **do

Select the global best from the Pareto front using roulette-wheel selection

Update the direction of the particle as expressed through equation (3.5)

Update the position of the particle as expressed through equation (3.6)

Compute the fitness function expressed through equations (3.7) and (3.8)

Update the particle's personal best,

end for

Update the solutions of the Pareto front

end for

for** every particle in the Pareto front **do

Compute the IQLV*

end for

Determine the position of particle having maximum IQLV

Construct the final de-noised image

**The objective functions have been computed with LMMSE algorithm for first approach whereas objective functions have been computed with proposed NL-Kalman filtering for second approach*

3.5 Results and Discussion

The results of proposed de-noising Algorithm are presented here, and are compared with (i) Kalman filter and (ii) LMMSE filter utilizing noise estimation based on mode of local mean. The comparison has been quantified in terms of following image quality measures: (i) PSNR, (ii) AQI, (iii) IQLV and (iv) SSIM. These measures are capable of quantifying the level of de-noising and edge preservation in an image. Figure 3.1 shows the comparison of standard LMMSE and proposed MOPSO-LMMSE algorithms. The present experiment has considered 50 number of iterations for both of these algorithms. The results shown in this figure are the mean and standard deviation values corresponding to the different level of noise for five T1 weighted and T2 weighted MRI dataset images. The present study also analyses the MOPSO led noise estimation qualitatively. For this purpose, the 90^{th} slice of T1 weighted ground truth image added with noise σ_n =15 and the effectiveness of these two methods has been shown. Fig. 3.2 (c) and Fig. 3.2 (d) shows the resultant images obtained from standard LMMSE filter and proposed MOPSO-LMMSE filter respectively. It can be clearly noted that the multiple sclerosis lesions are better visualized with the help of proposed MOPSO-LMMSE filter approach. It is also worth to mention that the proposed MOPSO based noise estimation is adaptive and this filter approach is able to better in comparison to classical approach which follows the assumption of Rician noise model after first iteration.

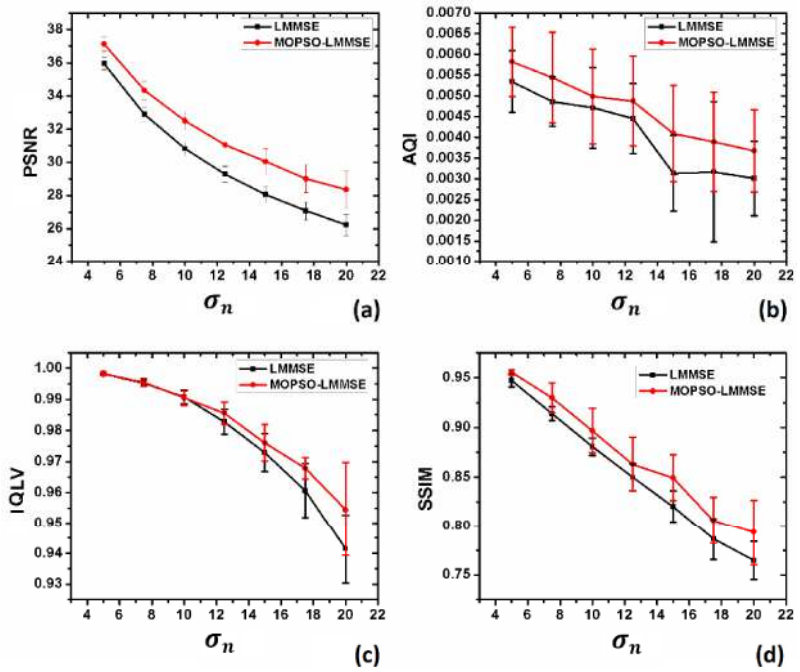

Figure 3-1: The comparison of classical recursive LMMSE (shown in black line) and proposed MOPSO-LMMSE (shown in red line) algorithms in terms of (a) noise vs. PSNR, (b) noise vs. Anisotropy, (c) noise vs. IQLV, and (d) noise vs. SSIM

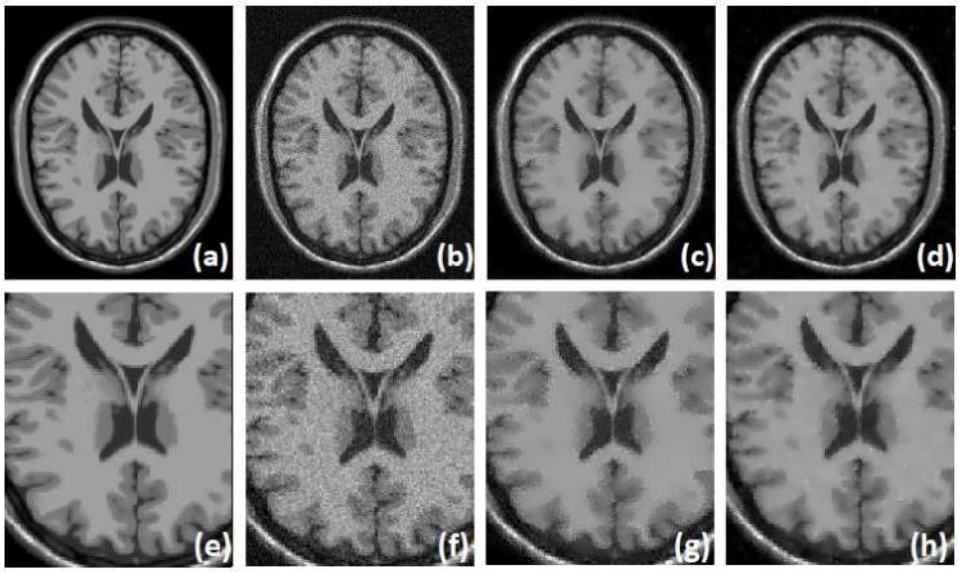

Figure 3-2: Qualitative comparison of the recursive LMMSE filter and proposed MOPSO-LMMSE filter (a) ground truth image, (b) ground truth image affected by noise with $\sigma_n = 15$, (c) standard LMMSE filtered image and (d) proposed MOPSO-LMMSE filter. The second row (e-h) shows the zoomed section of respective first row images.

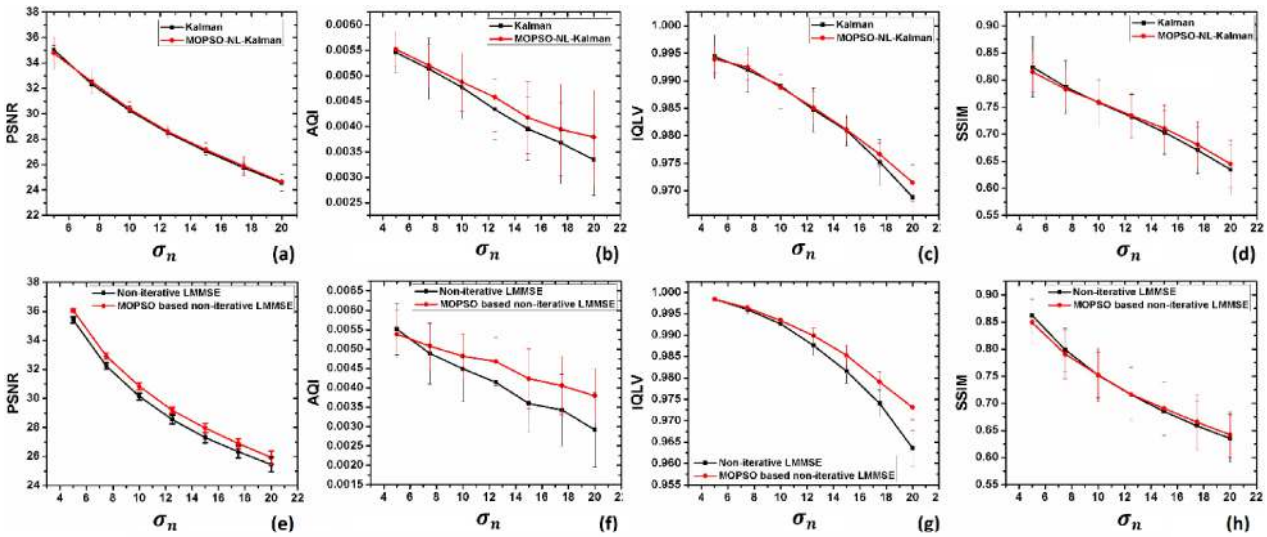

Figure 3-3: Comparison of standard non-iterative Kalman filter vs. non-iterative MOPSO-NL-Kalman and non-iterative LMMSE (shown in black line) vs. non-iterative MOPSO-LMMSE (shown in red line) in terms of (a, e) PSNR, (b, f) AQI, (c, g) IQLV and (d, h) SSIM

Further, the effectiveness of proposed MOPSO based noise estimation approach has been tested when filtering has been performed non-iteratively. The present study proposed non-local statistics based Kalman filter, which de-noises the MRI data in a single iteration. This proposed approach (MOPSO-NL-Kalman filter) has been compared with classical Kalman filter. The study has also included the comparison of non-iterative standard LMMSE filter, and non-iterative MOPSO-LMMSE filter. Figure 3.3 shows the quantitative performance of these two non-iterative filters in terms of image quality measures. The results obtained by MOPSO based noise estimation approach in non-iterative filtering show that proposed approach is capable of producing better de-noised MRI data than the conventional approaches. The qualitative results are shown in Fig. 3.4 also support the later statement, where MOPSO led approach is showing better differentiation of gray matter and white matter along with superior visualization of infarcts.

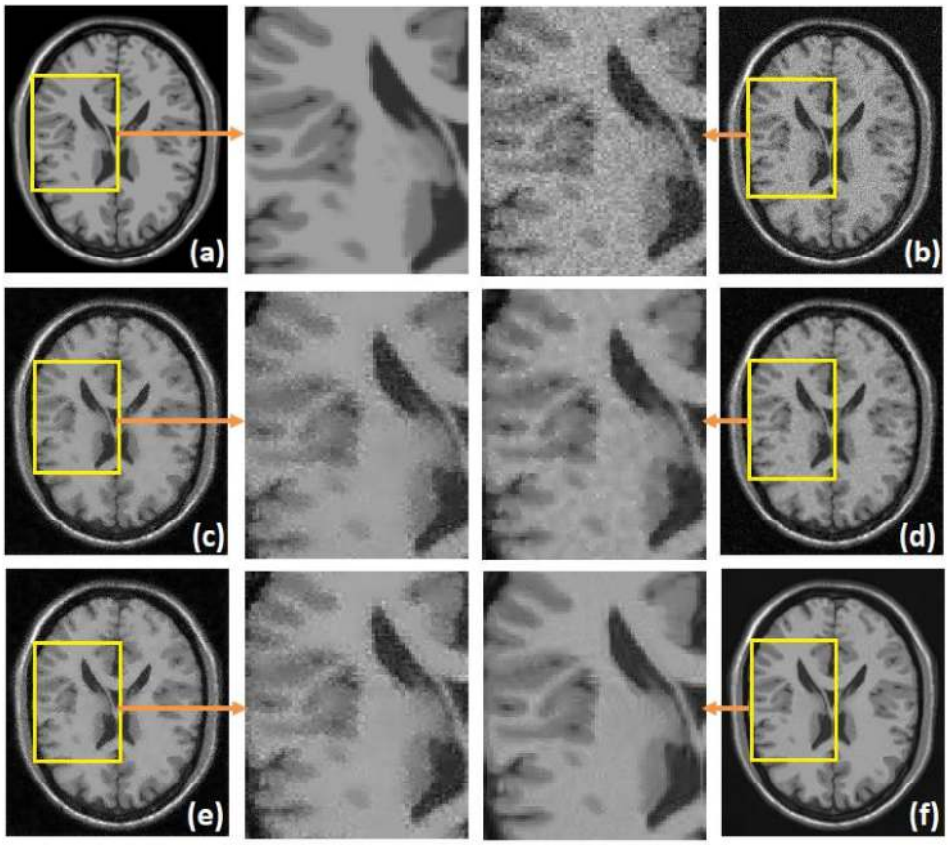

Figure 3-4: Comparison of classical non-iterative filters and MOPSO based noise estimation followed by non-iterative filters, (a) ground truth data, (b) ground truth data affected by noise with σ_n =15, filtered data processed with (c) standard LMMSE filter, (d) proposed MOPSO-LMMSE filter, (e) standard Kalman filter and (f) proposed MOPSO-NL-Kalman filter.

3.5.1 Proposed de-noising algorithms on real MRI data

This section shows the effectiveness of proposed algorithms on real MRI data. Figure 3.5 shows T2 and Fluid-attenuated inversion recovery (FLAIR) sequences of MRI of the same patient, who was suspicious of white matter lesion. As ground truth data is not available in real cases, the new fitness functions have been implemented based on non-referential image quality indexes, i.e., image content matrix (ICM) [142] and AQI. The ICM is correlated with the noise level, contrast, and sharpness of the structured regions. These two measures yield the non-dominant set of solutions. Further, the dominant solution has been obtained

corresponding to highest contrast enhancement factor [143], which helps to obtain a better contrast of lesion. Figure 3.5 has shown the de-noising results of proposed MOPSO-LMMSE filter and MOPSO-NL-Kalman filter.

The de-noised images are showing a better depiction of subtle white matter lesions. On unbiased blinded clinical reading of both group of images, consistently the lesions were labeled as "*suspicious*" in the native category while "*confirmed*" in the MOPSO-NL-Kalman de-noised category.

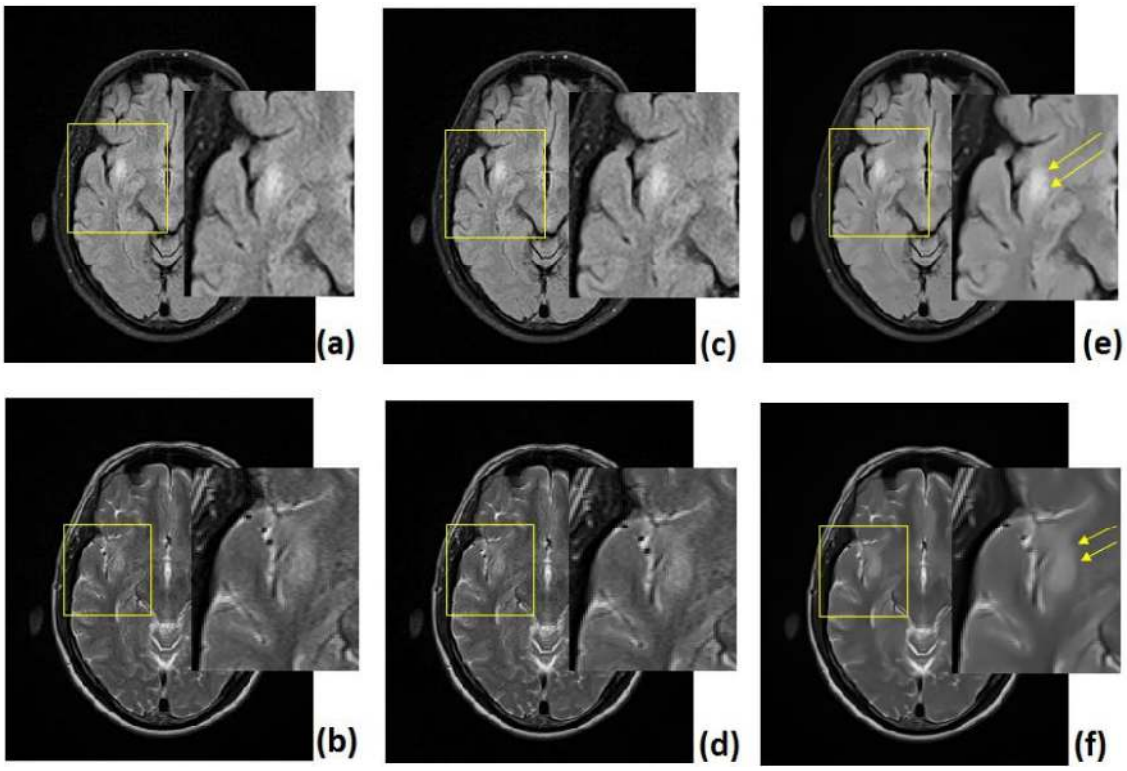

Figure 3-5: (a) T2 sequence of MRI (having resolution: 512×448, echo time: 97, repetition time: 4500, field of view=195×230), and (b) FLAIR sequence of MRI (having resolution: 512×448, echo time: 89, repetition time: 7200, inversion time: 2250, field of view=320×272) suspicious of white matter lesion. (c,d) Resultant data obtained from the proposed MOPSO-LMMSE filter, and (e,f) resultant data obtained from the proposed MOPSO-NL-Kalman filter

3.5.2 Comparison of proposed de-noising algorithms with standard algorithms

The de-noising/enhancement of MRI data primarily improves the visual perception and has the positive influence on the decision of the radiologists. The proposed MOPSO-NL-Kalman filter and proposed MOPSO-LMMSE filter have been compared with the following standard filters. (i) The Wiener filter [113], where the size of window has been kept five. (ii) Wavelet filter [36], while adopting bi-orthogonal 6.8 wavelet and three decomposition levels. (iii) NLM filter [24], where the search window has been kept seven and similarity window five. (iv) The local statistics based Kalman filter [121], where the size window has been kept seven and number of iterations fifty. (v) Recursive and non-recursive standard LMMSE filtering [27], where the size window has been kept seven. The number of iterations has been kept fifty and one respectively for recursive and non-recursive LMMSE filtering. These de-noising algorithms are chosen in the present study as they are popular and appreciated for the de-noising of MRI data.

Another aspect of MRI image analysis is a computer-aided diagnosis, where the performance of segmentation along with enhancement is equally essential. Apart from filtering performance, segmentation results include shape, gray-level difference and spatial distance of pixels. Hence, following the de-noising, this data is used as the input to the segmentation using enhanced fuzzy c-means (EnFCM) algorithm. Figure 3.6 shows the qualitative comparison of visual image quality produced by different de-noising methods on T1 weighted simulated standard data. This figure also shows the segmentation results produced by filtering followed by EnFCM. Further, the present study shows the qualitative comparison of de-noising and segmentation on real MRI data. In this view, a case of suspicion of pituitary microadenoma has been considered, where dynamic contrast-enhanced (DCE)

sequence of MRI has been selected for the analysis. Figure 3.7 shows de-noised DCE-MRI data obtained from previously proposed standard algorithms and proposed filtering algorithms. The cropped enlarged view of segmented pituitary gland shows the microadenoma region in gray pixel and normal region in white pixel. The effect of noise can be seen on segmentation results in case of Weiner and wavelet filters, whereas conventional Kalman filter based de-noising produced blurring effect and hence produced inaccurate segmentation of microadenoma. It can be noted from the figure that microadenoma can precisely visualized and segment out with the help of proposed MOPSO-NL-Kalman filter.

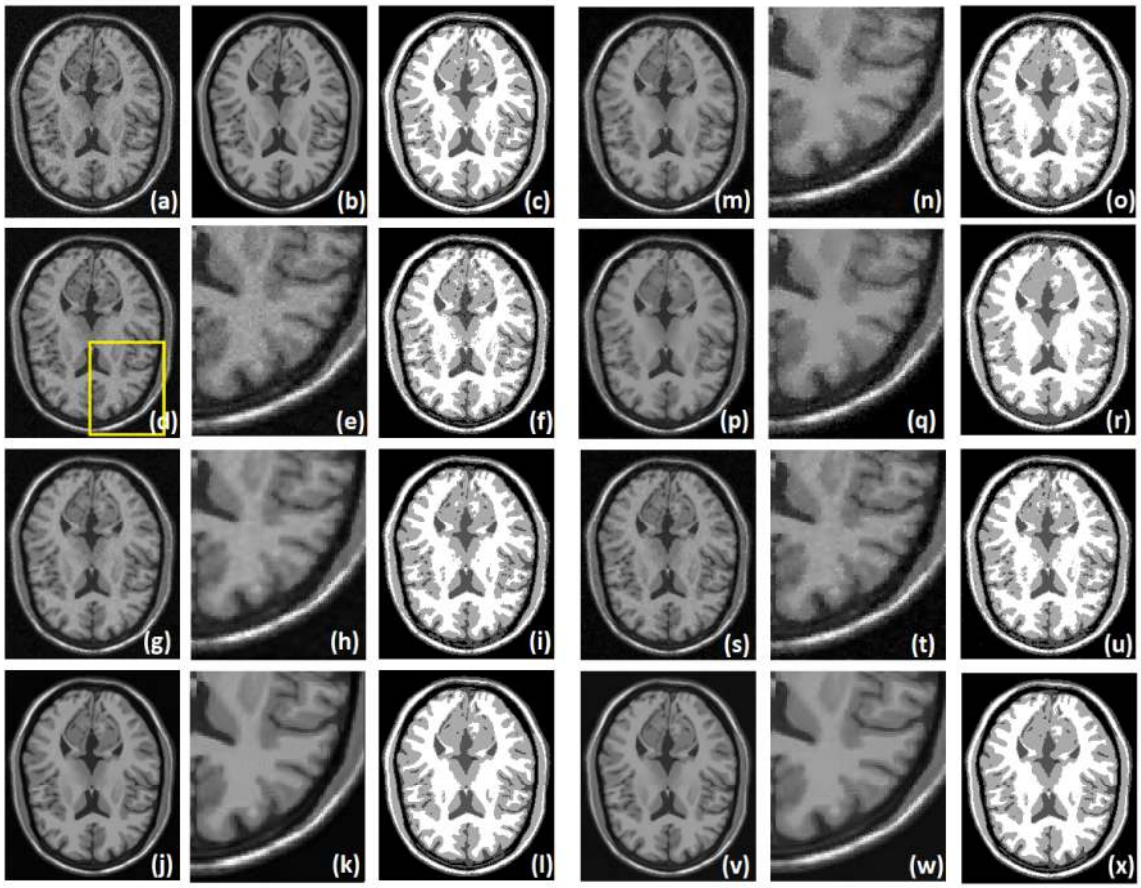

Figure 3-6: Comparison of de-noising and de-nosing followed by EnFCM segmentation for 80th slice of T1 dataset image, (a) ground truth data corrupted by noise with σ_n =12.5, (b) ground truth data, (c) ground truth segmentation. The de-noised data, zoomed section and segmented data for (d-f) wavelet-based filter, (g-i) Wiener

filter, (j-l) NLM filter, (m-o) Kalman filter, (p-r) LMMSE filter, (s-u) proposed MOPSO-LMMSE filter and (v-x) proposed MOPSO-NL-Kalman filter

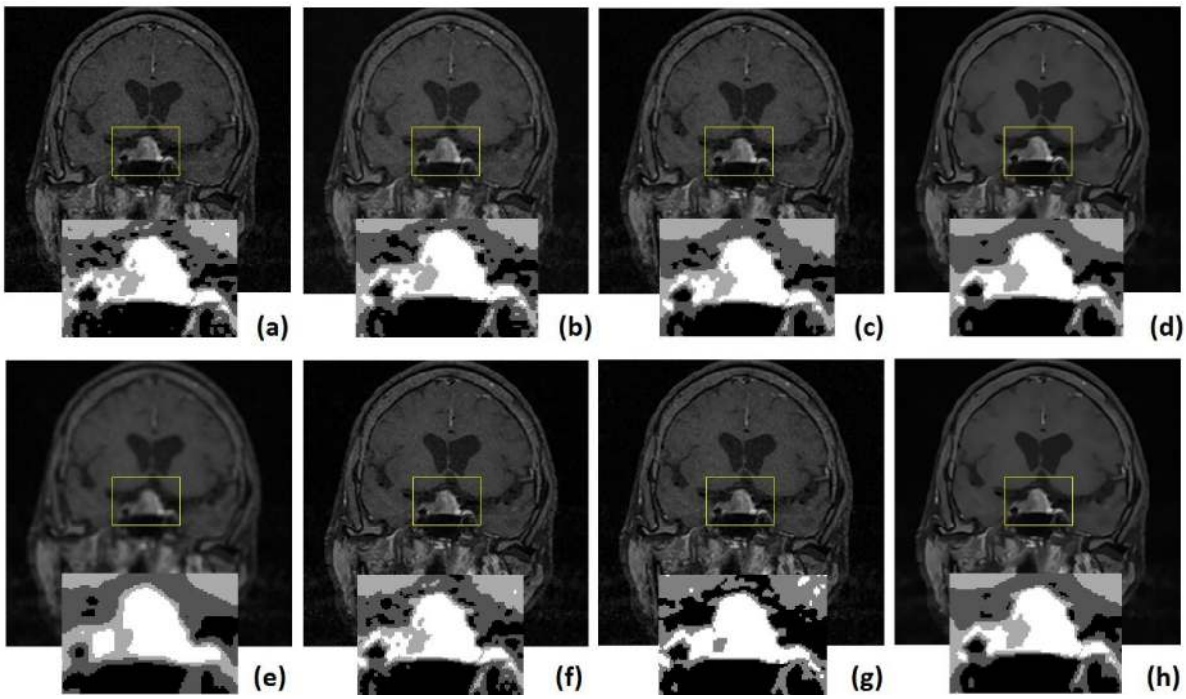

Figure 3-7: Comparison of de-noising results for real DCE-MRI data (having resolution: 384×384, echo time: 10, repetition time: 497). (a) Input MRI data, results obtained after applying (b) wavelet filter, (c) Wiener filter, (d) NLM filter, (e) Kalman filter, (f) LMMSE filter, (g) proposed MOPSO-LMMSE filter and (h) proposed MOPSO-NL-Kalman filter. The segmentation results obtained from de-nosing algorithms followed by EnFCM, the pituitary microadenoma has cropped from segmented brain MRI and its enlarged view has shown at bottom of each filtered image.

Table 3-2 shows the comparative performance of considered de-noising methods. The window size 7×7 and 50 number of iterations have been considered for both standard LMMSE and proposed MOPSO-LMMSE algorithms to make a fair comparison. Standard Kalman filter has been used the local statistics whereas the present study proposed Kalman filter based on non-local statistics. Table 3-2 reveals the edge of both proposed algorithms over the other previously proposed standard algorithms in terms of visual image quality and segmentation quality. It can determine from the table that the proposed MOPSO-LMMSE produces the better visual image quality of MRI data at the low-medium noise level, whereas

proposed MOPSO-NL-Kalman performs better if MRI data corrupted with the high noise level, i.e., σ_n =15 and more. Further, the proposed MOPSO-LMMSE gives slightly better segmentation quality at the low noise level, i.e., up to σ_n =7.5, whereas above this noise level proposed MOPSO-NL-Kalman gives the best segmentation accuracy.

Table 3-2: Performance evaluation of de-noising algorithms

Noise		Visual Image Quality						Segmentation Quality			
		PSNR		AQI		IQLV		JC		DI	
'σ_n'	Methods	Mean	STD	Mean	STD	Mean	STD	Mean	STD	Mean	STD
	Wavelet	34.287	0.526	0.0046	0.001	0.990	0.001	0.950	0.014	0.974	0.007
	Wiener	33.052	1.513	0.0044	0.000	0.967	0.016	0.936	0.025	0.967	0.013
	NLM	32.793	1.247	0.0051	0.001	0.986	0.006	0.916	0.029	0.956	0.015
	Kalman	34.699	0.757	0.0052	0.000	0.994	0.003	0.942	0.019	0.970	0.010
	LMMSE	36.123	0.249	0.0050	0.001	0.998	0.000	0.954	0.012	0.977	0.006
	MOPSO-LMMSE	**37.273**	0.230	**0.0054**	0.001	**0.998**	0.000	**0.957**	0.010	**0.978**	0.005
5	**MOPSO-NL-Kalman**	34.876	1.102	0.0052	0.000	0.994	0.003	0.942	0.021	0.970	0.011
	Wavelet	31.537	0.395	0.0044	0.000	0.989	0.001	0.939	0.015	0.969	0.008
	Wiener	30.956	1.084	0.0040	0.000	0.963	0.016	0.930	0.024	0.964	0.013
	NLM	31.104	0.768	0.0048	0.000	0.984	0.005	0.914	0.027	0.955	0.015
	Kalman	32.225	0.482	0.0048	0.000	0.991	0.003	0.937	0.014	0.967	0.007
	LMMSE	33.087	0.233	0.0044	0.001	0.995	0.001	0.933	0.017	0.965	0.009
	MOPSO-LMMSE	**34.522**	0.233	**0.0053**	0.001	**0.996**	0.001	**0.942**	0.014	**0.970**	0.008
7.5	**MOPSO-NL-Kalman**	32.526	0.886	0.0049	0.000	0.993	0.002	0.939	0.016	0.969	0.008
	Wavelet	29.077	0.314	0.0041	0.000	0.987	0.001	0.922	0.018	0.959	0.010
10	Wiener	29.110	0.836	0.0036	0.000	0.958	0.018	0.922	0.022	0.959	0.012

	NLM	29.481	0.498	0.0044	0.000	0.981	0.005	0.911	0.025	0.953	0.014
	Kalman	30.188	0.453	0.0045	0.000	0.989	0.003	0.927	0.015	0.962	0.008
	LMMSE	30.981	0.179	0.0043	0.001	0.991	0.002	0.909	0.021	0.952	0.012
	MOPSO-LMMSE	**32.653**	0.260	**0.0046**	0.001	**0.991**	0.003	0.925	0.016	0.961	0.009
	MOPSO-NL-Kalman	30.315	0.670	0.0046	0.000	0.989	0.003	**0.928**	0.015	**0.963**	0.008
	Wavelet	26.998	0.262	0.0039	0.000	0.984	0.002	0.898	0.023	0.946	0.013
	Wiener	27.509	0.701	0.0035	0.000	0.952	0.018	0.907	0.026	0.951	0.014
	NLM	27.977	0.402	0.0042	0.000	0.974	0.007	0.904	0.025	0.950	0.014
	Kalman	28.440	0.447	0.0042	0.000	0.984	0.003	0.914	0.016	0.955	0.009
	LMMSE	29.456	0.190	0.0041	0.001	0.983	0.004	0.883	0.025	0.938	0.014
	MOPSO-LMMSE	**31.180**	0.358	**0.0045**	0.001	**0.985**	0.003	0.909	0.020	0.952	0.011
12.5	**MOPSO-NL-Kalman**	28.506	0.612	0.0043	0.000	0.985	0.003	**0.917**	0.018	**0.957**	0.010
	Wavelet	25.251	0.232	0.0035	0.000	0.979	0.002	0.873	0.028	0.932	0.016
	Wiener	25.883	0.581	0.0031	0.000	0.944	0.019	0.893	0.032	0.943	0.018
	NLM	26.636	0.315	0.0039	0.000	0.972	0.006	0.900	0.026	0.947	0.015
	Kalman	26.949	0.458	0.0038	0.000	0.981	0.003	0.904	0.022	0.949	0.012
	LMMSE	28.200	0.235	0.0028	0.000	0.973	0.006	0.862	0.030	0.926	0.017
	MOPSO-LMMSE	**30.158**	0.553	0.0036	0.001	0.976	0.005	0.896	0.023	0.945	0.013
15	**MOPSO-NL-Kalman**	27.054	0.707	**0.0039**	0.000	**0.981**	0.003	**0.908**	0.021	**0.952**	0.012
	Wavelet	23.751	0.241	0.0033	0.000	0.969	0.005	0.836	0.036	0.910	0.021
	Wiener	25.124	0.966	0.0031	0.000	0.941	0.020	0.886	0.026	0.939	0.015
	NLM	25.398	0.347	0.0036	0.000	0.965	0.009	0.888	0.027	0.941	0.015
	Kalman	28.197	0.382	0.0032	0.001	0.964	0.009	0.859	0.028	0.924	0.016
17.5	LMMSE	25.600	0.624	0.0035	0.000	0.976	0.006	0.883	0.024	0.938	0.014

	MOPSO-LMMSE	**29.073**	0.700	0.0035	0.001	0.970	0.007	0.884	0.026	0.938	0.015
	MOPSO-NL-Kalman	25.753	0.885	**0.0037**	0.000	**0.977**	0.003	**0.891**	0.023	**0.942**	0.013
	Wavelet	22.433	0.195	0.0029	0.000	0.952	0.011	0.793	0.040	0.884	0.025
	Wiener	23.752	0.497	0.0027	0.000	0.929	0.024	0.866	0.028	0.928	0.016
	NLM	24.228	0.330	0.0034	0.000	0.958	0.009	0.878	0.024	0.935	0.013
	Kalman	24.361	0.790	0.0032	0.000	0.972	0.007	0.863	0.023	0.926	0.013
	LMMSE	26.359	0.349	0.0027	0.001	0.942	0.012	0.816	0.037	0.899	0.022
	MOPSO-LMMSE	**28.507**	0.878	0.0032	0.001	0.952	0.013	0.871	0.029	0.931	0.016
20	**MOPSO-NL-Kalman**	24.503	0.955	**0.0035**	0.000	**0.972**	0.004	**0.873**	0.024	**0.932**	0.014

3.6 Conclusions

The study has presented the MOPSO based noise estimation approach in combination with LMMSE filter and non-local Kalman filter. The effectiveness of proposed MOPSO based noise estimation approach has been demonstrated. First, MOPSO has been employed on the recursive LMMSE filter and compared with estimation based on mode of local mean followed by recursive LMMSE filter. The proposed MOPSO based noise estimation has been found highly valuable for recursive filters. Further, MOPSO based estimation has been employed on non-local Kalman filter, which is a non-recursive filter. The proposed MOPSO-NL-Kalman filter has been compared with standard Kalman filter, and MOPSO based non-recursive LMMSE filter has been compared with estimation based on mode of local mean followed by non-recursive LMMSE filter. Finally, the proposed algorithms have been compared with standard de-noising algorithms such as Wavelet, Wiener and NLM. The results show that the proposed de-noising algorithms performed better in terms of visual

image quality and segmentation accuracy. The presented de-nosing approaches have positive influence on diagnosis and segmentation results. The present study can conclude that the MOPSO-LMMSE is more effective for MRI data corrupted with the low-medium noise level, whereas MOPSO-NL-Kalman has been found valuable for MRI data corrupted with the high noise level.